


Article

Fault Detection-Based Multiple Local Manifold Learning and Its Application to Blast Furnace Ironmaking Process

Ke Wang¹, Ping Wu^{1,*}, Siwei Lou², Haipeng Pan¹  and Jinfeng Gao¹

¹ School of Information Science and Engineering, Zhejiang Sci-Tech University, Hangzhou 310018, China; 202120604129@mails.zstu.edu.cn (K.W.); jfgao@zstu.edu.cn (J.G.)

² College of Control Science and Engineering, Zhejiang University, Hangzhou 310027, China; swlou@zju.edu.cn

* Correspondence: pingwu@zstu.edu.cn

Abstract: Process safety plays a vital role in the modern process industry. To prevent undesired accidents caused by malfunctions or other disturbances in complex industrial processes, considerable attention has been paid to data-driven fault detection techniques. To explore the underlying manifold structure, manifold learning methods including Laplacian eigenmaps, locally linear embedding, and Hessian eigenmaps have been utilized in data-driven fault detection. However, only the partial local structure information is extracted from the aforementioned methods. This paper proposes fused local manifold learning (FLML), which synthesizes the typical manifold learning methods to find the underlying manifold structure from different angles. A more comprehensive local structure is discovered under a unified framework by constructing an objection optimization function for process data dimension reduction. The proposed method takes advantage of different manifold learning methods. Based on the proposed dimension reduction method, a new data-driven fault detection method is developed. Hotelling's T^2 and Q statistics are established for the purpose of fault detection. Experiments on an industrial benchmark Tennessee Eastman process whose average MDR and average FAR of FLML T^2 are 7.58% and 0.21% and a real blast furnace ironmaking process whose MDR and FAR of FLML T^2 are 2.80% and 0.00% are carried out to demonstrate the superiority and effectiveness of the proposed method.



Citation: Wang, K.; Wu, P.; Lou, S.; Pan, H.; Gao, J. Fault Detection-Based Multiple Local Manifold Learning and Its Application to Blast Furnace Ironmaking Process. *Electronics* **2023**, *12*, 4773. <https://doi.org/10.3390/electronics12234773>

Academic Editors: Qing-Guo Wang, Zhuoyun Nie, Chunjie Yang, Ping Zhou and Zhaohui Jiang

Received: 25 September 2023

Revised: 18 November 2023

Accepted: 21 November 2023

Published: 24 November 2023



Copyright: © 2023 by the authors. Licensee MDPI, Basel, Switzerland. This article is an open access article distributed under the terms and conditions of the Creative Commons Attribution (CC BY) license (<https://creativecommons.org/licenses/by/4.0/>).

Keywords: data-driven method; fault detection; manifold learning; blast furnace ironmaking process

1. Introduction

Industrial processes are becoming more complex and their hazards to the environment are receiving increasing attention. Process safety is a non-negligible component of industrial processes, which comprises several steps such as hazard identification and analysis [1]. In particular, the identification and analysis of hazards is a key step in the prevention and mitigation of major process accidents.

In industrial processes, timely and accurately identifying abnormal operating conditions can prevent major accidents and improve operational efficiency, thus achieving compliance with environmental and safety regulations. Dynamic process monitoring for hazard/fault identification is already a trend in the future development of process safety and risk management [2]. The real-time monitoring of process operations to ensure safety measures is an essential step in the modern process industry [3].

Fault detection plays a pivotal role in guaranteeing operation safety and reducing downtime in complex industrial processes [4,5]. Broadly speaking, fault detection techniques can be categorized into three classes, model-based, knowledge-based, and data-driven based methods [6]. Model-based methods rely on the mathematical model. However, the mathematical model is often difficult or time-consuming to establish for complex industrial processes such as the blast furnace ironmaking process. For knowledge-based methods, the model is built from expert knowledge or qualitative information, which

limits its applications for complex industrial processes. Conversely, only the measured process variables are required for data-driven fault detection methods. Thus, data-driven techniques are more suitable and efficient for the fault detection of complex industrial processes [7]. With the advance of the sensor, communication, and computing technologies, large amounts of data are collected in modern industrial processes. Under such circumstances, data-driven fault detection has gained an explosive amount of attention in recent years from academia and industry [8].

For data-driven methods, traditional multivariate analysis (MVA) and deep learning methods have gained considerable attention in the field of fault detection. The main advantage of deep learning methods is that they can learn the features of process data without feature engineering from deep neural networks. Deep learning methods have the powerful capability to capture the nonlinearity of process data through hierarchical abstraction. Recently, deep learning methods have been widely employed in fault detection and diagnosis. Wang et al. proposed a Bidirectional Gated Recurrent Unit (Bi-GRU) model for the fault diagnosis of Modular Multilevel Converters High Voltage DC (MMC-HVDC) [9]. Yu et al. proposed a graph-weighted reinforcement network (GWRNet) for the fault diagnosis of rotating machinery [10]. Velasco et al. developed a real-time anomaly detection intelligent system (RADIS) based on long short-term memory (LSTM) and a variational autoencoder (VAE) for the fault diagnosis of rotating machinery [11]. However, there exist some limitations in applying deep learning for fault detection and diagnosis such as large dataset requirements, computational resources, and poor interpretability.

To handle the highly correlated high-dimensional process data, multivariate analysis (MVA) has been widely employed in industrial processes [12]. In MVA, the process behavior is modeled by transforming the high-dimensional data into a lower-dimensional space. The features are extracted for establishing monitoring statistics. Among the MVA-based fault detection methods, principal component analysis (PCA) has gained widespread popularity in process monitoring and fault diagnosis in recent decades [13]. In PCA, process data are projected into a lower-dimensional space to preserve the significant variability information as much as possible. Due to its efficiency and simplicity, PCA has been successfully applied in a large number of industrial processes [14]. Despite this, PCA is regarded as a kind of globality-based linear dimensionality reduction technique. However, the process data mostly lie on or close to a low-dimensional manifold. Compared to globality-based methods, manifold learning is an approach to nonlinear dimensionality reduction which operates by discovering the manifold structure of data. In manifold learning, the input data are assumed to be sampled from a low-dimensional manifold. Representative manifold learning methods include Isomap [15], locally linear embedding (LLE) [16], Laplacian eigenmaps (LE) [17], local tangent space alignment (LTSA) [18], locality-preserving projections (LPPs) [19], neighborhood-preserving embedding (NPE) [20], and Hessian eigenmaps (or called Hessian LLE) [21].

In NPE, each data point is represented as a linear combination of the neighboring data points. Then, an optimal embedding is found to preserve the neighborhood structure in the dimensionality-reduced space [20]. Chen et al. [22] applied eigenvalue decomposition and generalized eigenvalue decomposition to solve the unstable problem caused by a singularity problem in NPE, and developed an NPE-based incipient fault detection method for small-scale cyber-physical systems. Since the NPE method can preserve the local manifold structure of different modes, Song et al. [23] performed NPE on the time-lagged variables for multimode dynamic process monitoring. LPP is designed to find the optimal linear approximations to the eigenfunctions of the Laplace Beltrami operator on the manifold through the nearest neighbor search in the low-dimensional space [19]. Duan et al. [24] employed LPP to preserve the local structure of process data, and then adopted a least squares support vector machine to predict the key-performance indicator. Zhang et al. [25] combined LPP and PCA to preserve both global and local structures of the dataset and developed a fault detection and identification method by utilizing the extracted features. LLE attempts to discover nonlinear structure in high-dimensional data by exploiting the

local symmetries of linear reconstructions [21]. Wu et al. learned structure information by LLE and incorporated the extracted local information into canonical correlation analysis (CCA) for quality-relevant nonlinear process monitoring [26]. Li and Zhang implemented the supervised locally linear embedding projection method for bearing fault diagnosis and illustrated its validity using the experimental data [27]. Different manifold learning methods focus on uncovering the manifold structure with different criteria. They rely on the knowledge and experience of experts for their own purposes. Therefore, only partial information from the underlying manifold is learned by each existing local manifold learning method. Although there are many other manifold learning methods, LE, LLE, and HLLE are easily fused to characterize the geometric information of the manifold from different perspectives under the framework of the local tangent coordinate system. To take advantage of different manifold learning methods to better uncover the underlying manifold structure, Xing et al. [28] provided a common framework to synthesize the partial information extracted from different local manifold learning methods under local tangent coordinates.

Motivated by the above discussions, a novel data-driven fault detection based on FLML is proposed in this paper. In the proposed FLML, the partial information on the geometric structure of the underlying manifold is firstly extracted from LE, LLE, and Hessian locally linear embedding (HLLE) methods, respectively. A novel objective function is formulated to fuse the extracted partial information. On the basis of the optimization results, FLML can learn the geometric information from different local methods. The geometric structure of the underlying manifold is more thoroughly explored by the proposed FLML, compared to LE, LLE, and HLLE. In the proposed FLML method, the richer local information can be exploited by taking the data proximity, local linear relationships, and local Hessian structures into account simultaneously. On the other hand, the proposed FLML can manifest robustness due to the local information extracted from different views. Compared to the method developed in [28], which requires the determination of fusion coefficients, only the global embedding coordinates are obtained in the proposed FLML. Thus, the proposed FLML method is simpler. Like the PCA-based fault detection method, two monitoring statistics including Hotelling's T^2 and Q statistics are established. The effectiveness and advantages of the proposed FLML-based fault detection are illustrated by an industrial Tennessee Eastman process benchmark and a real blast furnace ironmaking process.

The rest of this paper is organized as follows. Section 2 briefly introduces the ideas of LE, LLE, and HLLE. Section 3 illustrates the proposed FLML method and its application in fault detection in detail. In Section 4, the proposed FLML-based fault detection approach is verified through an industrial Tennessee Eastman (TE) process benchmark and a real blast furnace ironmaking process. Finally, Section 5 provides the conclusion.

2. Brief Review of LE, LLE, and HLLE

2.1. LE

LE is a well-known manifold learning method to extract local structure features in the original sample space. The main idea behind LE is that the corresponding projections of neighboring points in the low-dimensional space should be close if the neighboring points in the high-dimensional space are close [17].

Given a set $\mathbf{X} = [x_1, x_2, \dots, x_n]^T \in \mathbb{R}^{n \times D}$ of n sample points in \mathbb{R}^D , where D is the number of variables. The goal of LE is to find a set of points $\mathbf{Y} = [y_1, y_2, \dots, y_n]^T \in \mathbb{R}^{n \times d}$ ($d \ll D$) in the low-dimensional space to have the neighbor relations between sample points \mathbf{X} in the high-dimensional space.

In LE, the first step is to construct the adjacency graph. k -nearest neighbors (KNN) is a widely used neighbors selection strategy, due to its simplicity. To model the neighborhood relations between sample points, an adjacency matrix $\mathbf{S} \in \mathbb{R}^{n \times n}$ is employed, where each element S_{ij} represents the neighborhood relations between x_i and its neighbor x_j . Using the Gaussian heat kernel, the adjacency matrix S_{ij} can be formed as follows:

$$S_{ij} = \begin{cases} e^{-\|x_i - x_j\|^2 / 2\delta^2}, & x_i \text{ and } x_j \in \text{neighbors} \\ 0 & , \text{ otherwise} \end{cases} \tag{1}$$

where δ is the kernel width.

The objective function of LE can be cast as

$$\begin{aligned} \min_{\mathbf{Y}} \quad & J_{LE} = \sum_{i,j=1}^n \|\mathbf{y}_i - \mathbf{y}_j\|^2 S_{ij} = \mathbf{Y}^T \mathcal{L}_e \mathbf{Y} \\ \text{s.t.} \quad & \mathbf{Y}^T \mathbf{D} \mathbf{Y} = \mathbf{I} \end{aligned} \tag{2}$$

where \mathbf{D} ($D_{ii} = \sum_{j=1}^n S_{ij}$) is a diagonal matrix, and \mathcal{L}_e ($\mathcal{L}_e = \mathbf{D} - \mathbf{S}$) is defined as a Laplacian matrix.

The optimization problem (2) is equivalent to generalized eigenvalue problem,

$$\mathcal{L}_e \mathbf{Y} = \lambda \mathbf{D} \mathbf{Y} \tag{3}$$

It can be readily solved through eigenvalue decomposition.

2.2. LLE

In LLE, the key assumption is that each data point and its neighbors are lied on or closed to a locally linear patch. A sample can be represented as the linear combination of multiple samples from its neighborhood [16]. The optimization problem of LLE can be formulated as

$$\begin{aligned} \min_{\theta_{ij}} \quad & J_{LLE} = \sum_{i=1}^n \|\mathbf{x}_i - \sum_{j=1}^n \theta_{ij} \mathbf{x}_j\|^2 \\ \text{s.t.} \quad & \sum_{j=1}^n \theta_{ij} = 1 \end{aligned} \tag{4}$$

where θ_{ij} is the weight coefficient and only when \mathbf{x}_i and \mathbf{x}_j are neighbors the corresponding θ_{ij} has a value, otherwise it is 0. Similarly, the neighbors selection can be determined by the KNN method.

The low-dimensional features denoted as $\Phi = [\phi_1^T, \phi_2^T, \dots, \phi_n^T]^T$, the minimization problem (4) can be formulated as

$$\begin{aligned} \min_{\Phi} \quad & J_{LLE} = \sum_{i=1}^n \|\phi_i - \sum_{j=1}^n \theta_{ij} \phi_j\|^2 = \text{tr}(\Phi^T \mathcal{L}_l \Phi) \\ \text{s.t.} \quad & \Phi^T \Phi = \mathbf{I} \end{aligned} \tag{5}$$

where \mathbf{I} is the identity matrix, $\Theta = [\theta_{ij}]_{i=1, \dots, n, j=1, \dots, n}$ is the weight coefficient matrix, and $\mathcal{L}_l = (\mathbf{I} - \Theta)^T (\mathbf{I} - \Theta)$.

Similarly, the optimization problem (5) can be solved through eigenvalue decomposition.

2.3. HLLE

HLLE is regarded as a variant of LLE. Assume that the low-dimensional data representation is locally isometric to an open and connected subset, the idea behind HLLE is to minimize the curviness of the high-dimensional manifold while embedding it into a low-dimensional space [21].

Assume that the set $\mathbf{X} = [\mathbf{x}_1, \mathbf{x}_2, \dots, \mathbf{x}_n]^T \in \mathbb{R}^{n \times D}$ is located on a smooth manifold $\mathcal{M} \subset \mathbb{R}^D$ with an intrinsic dimension $d \ll D$; PCA is firstly performed on \mathbf{X} to obtain d eigenvectors $\mathbf{V} = [\mathbf{v}_1, \mathbf{v}_2, \dots, \mathbf{v}_d] \in \mathbb{R}^{D \times d}$.

It is assumed that the number of neighbors of the sample x_i is k . Then, the local tangent coordinate $u_j, j = 1, \dots, k$ of the sample x_i can be calculated by projecting the local neighborhood into the tangent subspace

$$u_j^i = \langle V, x_j - x_i \rangle = V^T(x_j - x_i) \tag{6}$$

Then, the Hessian matrix H^i containing local information will be calculated by the projection of neighbors x_j in the tangent coordinate u_j . By defining $U^i = [U_1^i, U_2^i, \dots, U_k^i]$ constructed by the u_j^i [29], H^i can be constructed by the last $(U^i)^\dagger$ where $(\cdot)^\dagger$ is the pseudo-inverse symbol. Therefore, the local objective of HLLE can be estimated with

$$\begin{aligned} \min_{f^i} J_{HLLE} &= \frac{1}{N} \sum_{i=1}^N f^{iT} H^{iT} H^i f^i \\ \text{s.t. } f^{iT} f^i &= 1 \end{aligned} \tag{7}$$

where $f^i = [f(x_1), f(x_2), \dots, f(x_k)]^T$ is the local projection and $f(x_j), j = 1, \dots, k$ is the smooth function used to estimate the local neighborhood information at a fixed point x_i . Then, extending the local neighborhood information to all samples, we can obtain the global projection $f = [f^1, f^2, \dots, f^N]^T$. The optimization objective of HLLE can be rewritten as

$$\begin{aligned} \min_f J_{HLLE} &= \frac{1}{N} \sum_{i=1}^N f^T S^{iT} H^{iT} H^i S^i f \\ &= \text{tr}(f^T \mathcal{L}_h f) \\ \text{s.t. } f^T f &= 1 \end{aligned} \tag{8}$$

where $\mathcal{L}_h = \frac{1}{N} \sum_{i=1}^N S^{iT} H^{iT} H^i S^i$ is the local objective and the neighboring selection matrix S^i can convert local projection to global projection $f^i = S^i f$ and each entry S_{ij}^i of S^i can be obtained as

$$S_{ij}^i = \begin{cases} 1, & x_i \text{ and } x_j \in \text{neighbors} \\ 0, & \text{Otherwise} \end{cases} \tag{9}$$

For solving the above optimization problem (8), eigenvalue decomposition is also utilized. Details of HLLE can be found in [21].

3. Proposed Method

3.1. FLML: Fused Local Manifold Learning

From the previous section, it can be found that LE, LLE, and HLLE can explore the local geometric structure information from different perspectives. To synthesize this local information, Xing et al. [28] fused the local information obtained by multiple manifold learning methods including LE, LLE, HLLE, and LTSA by reformulating the different local manifold algorithms under the local tangent coordinate system to reveal the underlying manifold of the dataset. Similar to [28], the fused local objective \mathcal{F}_f is defined as

$$\mathcal{F}_f = c_1 \mathcal{L}_e + c_2 \mathcal{L}_l + (1 - c_1 - c_2) \mathcal{L}_h \tag{10}$$

to integrate LE, LLE, and HLLE. Here, $c_1 + c_2 \leq 1, c_1, c_2 \in [0, 1]$ are the fusion coefficients.

Remark 1. In [28], the local objectives are optimized to determine the fusion coefficients and global embedding coordinates simultaneously. In addition, there is another required hyperparameter "power parameter". In [30], the selection of c is determined by employing the alternating optimization method which iteratively updates c and Y in an alternating fashion. Therefore, the optimization procedure may be cumbersome. For simplicity, only the global embedding coordinates are obtained in this study. The fusion coefficients are considered fixed values. In this study, our main goal is to develop a fault detection method by fusing LE, LLE, and HLLE to extract the local structure of

process data with richer information in dimension reduction. Therefore, the optimization procedure of the proposed FLML approach is much simpler in this study.

Similar to LE, LLE, and HLLLE, the proposed FLML method is a kind of linear projection method. To facilitate the online fault detection, an explicit linear mapping from the original space to the low-dimensional space is provided. Thus, the main goal of FLML is to seek a transformation matrix that maps the high-dimensional data to low-dimensional data. Suppose that $w \in \mathbb{R}^{D \times 1}$ is the transformation vector from X to y ; therefore, the projections in the low-dimensional space can be represented as $y = w^T X$.

To synthesize the local geometric structure information and impose constraints to prevent multiple solutions, the objective function of FLML is formulated as follows:

$$\begin{aligned} \min_w \quad & J_{FLML} = w^T X^T \mathcal{F}_f X w \\ \text{s.t.} \quad & w^T X^T X w = 1 \end{aligned} \tag{11}$$

Remark 2. As shown in (10) and (11), it is noticed that the corresponding local structure will be extracted from LE, LLE, and HLLLE while c_1 and c_2 are selected to be $(c_1 = 1, c_2 = 0)$, $(c_1 = 0, c_2 = 1)$ and $(c_1 = 0, c_2 = 0)$, respectively.

To solve the optimization problem (11), we use the technique of Lagrange multipliers as follows:

$$J_{FLML} = w^T X^T \mathcal{F}_f X w + \lambda / 2 (1 - w^T X^T X w) \tag{12}$$

where λ is the Lagrange multiplier.

While $\frac{\partial J_{FLML}}{\partial w} = 0$, it results in

$$X^T \mathcal{F}_f X w = \lambda X^T X w \tag{13}$$

Hence, we can use generalized eigenvalue decomposition to obtain the transformation vector w from (13). Finally, the transformation matrix $W \in \mathbb{R}^{D \times d}$ can be assembled by the eigenvectors corresponding to the smallest d eigenvalues derived from the result of generalized eigenvalue decomposition.

3.2. FLML-Based Fault Detection

Generally, data-driven fault detection methods contain two steps, namely offline modeling and online monitoring. In the offline modeling step, the process data $X \in \mathbb{R}^{n \times D}$ are collected under normal operating conditions for training. Using the training data X , an FLML model is established. Subsequently, the low-dimensional data $Y \in \mathbb{R}^{n \times d}$ are obtained. With the transformation matrix W , the relation between X and Y can be represented as

$$Y = XW \tag{14}$$

The residual matrix $E \in \mathbb{R}^{n \times D}$ is

$$E = X - YW^T = X(I - WW^T) \tag{15}$$

In the online monitoring step, the low-dimensional data point y_{new} and residual e_{new} of a new standardized sample x_{new} is obtained:

$$\begin{cases} y_{new} = W^T x_{new} \\ e_{new} = (I - WW^T)x_{new} \end{cases} \tag{16}$$

The Hotelling's T^2 and squared prediction error (SPE) statistics (also called Q statistics) are often used for monitoring. For T^2 statistic, the Mahalanobis distance is used to evaluate the variations in \mathbf{y} . The Hotelling's T^2 statistic is defined as

$$T^2 = \mathbf{y}_{new}^T \mathbf{\Lambda}^{-1} \mathbf{y}_{new} \quad (17)$$

where $\mathbf{\Lambda}$ is the covariance matrix of \mathbf{Y} which is extracted from the normal operating condition data \mathbf{X} .

For Q statistic, the Euclidean distance is adopted to evaluate the magnitude of vector in the residual space as follows:

$$Q = \mathbf{e}_{new}^T \mathbf{e}_{new} \quad (18)$$

Under the assumption that all operating parameters and prediction errors have a Gaussian distribution, the upper control limits (UCLs) of Hotelling's T^2 and Q statistics are determined by means of F distribution and χ^2 distribution, respectively. Thus, with a level of significance α , the UCLs are calculated as follows:

$$\begin{cases} T_{UCL}^2 \sim \frac{d(n-1)}{n-d} F(d, n-d, \alpha) \\ Q_{UCL} \sim g\chi_{h,\alpha}^2 \end{cases} \quad (19)$$

where $g = \sigma^2/2\mu$ and $h = 2\mu^2/\sigma^2$, μ is the sample mean, and σ^2 is the sample variance of the statistic Q . g and h are calculated using normal operating condition data.

In FLML, the parameters such as the number of the neighbors k , the bandwidth δ of Gaussian heat kernel, the fusion weights c_1 and c_2 , and the number of latent variables d are determined by grid search method. The general procedure is elaborated as follows:

- Step 1 (k): The finding of neighborhood relations is related to the selection of k [26]. To balance the computation complexity and generalization capability, we choose k in the range of [1 : 10] with the smallest mean false alarm rate (FAR). The definition of FAR can be found in the next section.
- Step 2 (δ): If the bandwidth of the Gaussian heat kernel function is too small, the kernel will be sensitive to noise. A large bandwidth may create an overly smooth mapping [31]. Empirically, the bandwidth δ is chosen as $\delta = b m \sigma^2$ where m is the size of the variables, b is a constant, and σ^2 represents the variance in the data, which is 1 as the original data are normalized [25]. In the case studies, $b = 50$ are selected.
- Step 3 (c_1 and c_2): It is noticeable that the hyper-parameters c_1 and c_2 have an important influence on the performance of the proposed FLML method. However, it is challenging work to choose a set of optimal hyper-parameters. As a traditional way of performing hyper-parameter optimization, the grid search method is employed. For this purpose, a finite set of $c_1 \in \{0, 0.05, \dots, 0.95\}$ and $c_2 \in \{0, 0.05, \dots, 0.95\}$ are explored by minimizing the mean FAR.
- Step 4 (d): Similar to NPE-based and LPP-based methods, the number of latent variables d is selected by searching for eigenvalues similar to the smallest non-zero eigenvalue.

A scheme of the proposed fault detection method is provided as Figure 1, and the procedure is described as follows:

Offline training:

- Step 1. Standardize the collected dataset \mathbf{X} under normal operating conditions.
- Step 2. Extract the local structure information by calculating \mathcal{L}_e , \mathcal{L}_l and \mathcal{L}_h from (2), (5), and (8).
- Step 3. Establish the fused local structure \mathcal{F} defined in (10).
- Step 4. Perform eigenvalue decomposition as (13) to solve the optimization problem (11) and retain the eigenvectors corresponding to the smallest d eigenvalues as the transformation matrix \mathbf{W} .
- Step 5. Compute the UCLs T_{UCL}^2 and Q_{UCL} using (19).

Online monitoring:

- Step 1. Standardize a newly collected sample x_{new} .
- Step 2. Obtain the score y_{new} and residual e_{new} from (16).
- Step 3. Compute the online statistics T^2 and Q according to (17) and (18), respectively.
- Step 4. If the real-time T^2 or Q statistics are beyond the corresponding UCL, the alarm is triggered.

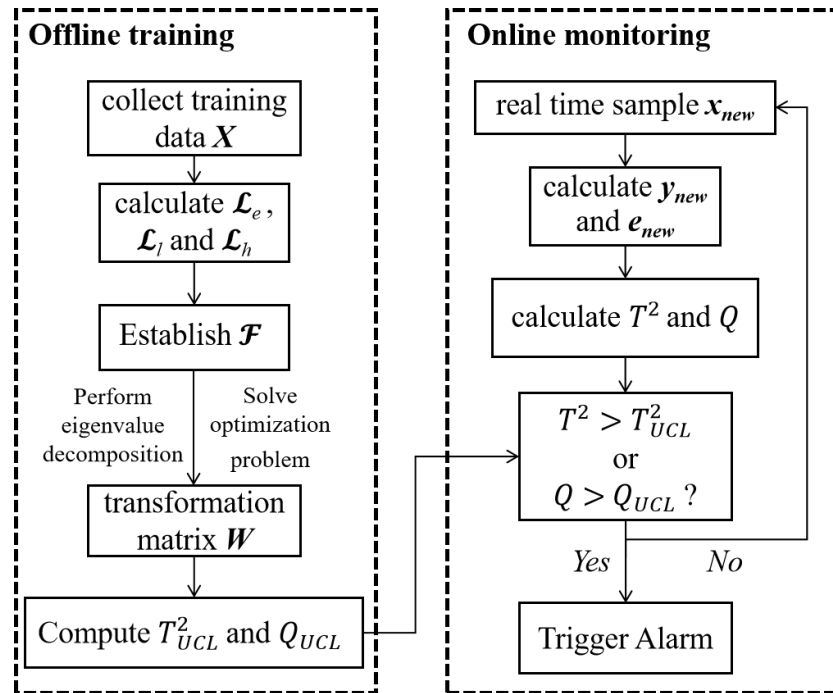


Figure 1. The scheme of the proposed fault detection method.

4. Case Studies

In this section, the proposed FLML-based fault detection method is verified by conducting experiments on the Tennessee Eastman process and a real-world blast furnace ironmaking process.

4.1. Tennessee Eastman Process

The TE process is a well-known and widely used industrial benchmark for comparing the performance of process monitoring and control [32]. In the TE process, there are five main units including a separator, a compressor, a reactor, a vapor/liquid separator, a stripper and a condenser, and eight components A-H. It also has 12 manipulated variables (XMV1-11) and 41 measured variables (XMEAS1-41). Among these variables, XMEAS (23–41) are the composition of A-H measured with 6 min sampling intervals in different positions. Other variables are collected with 3 min sampling intervals. There are 21 pre-programmed faults in the TE process. Of 21 faults, due to the absence of observable change in the mean and standard deviation between their corresponding faulty and normal operation, faults 3, 9, and 15 are very difficult to detect [33]. In this study, faults 3, 9, and 15 are ignored. The descriptions of the faults considered in this study are listed in Table 1.

Table 1. Faults description in the TE process.

No.	Fault Description	Fault Type
IDV(0)	Normal Situations	-
IDV(1)	A/C feed ratio, B composition constant (Stream 4)	Step
IDV(2)	B composition, A/C ratio constant (Stream 4)	Step
IDV(4)	Reactor cooling water inlet temperature	Step
IDV(5)	Condenser cooling water inlet temperature	Step
IDV(6)	A feed loss (Stream 1)	Step
IDV(7)	C header pressure loss-reduced availability (Stream 4)	Step
IDV(8)	A, B, C feed composition (Stream 4)	Random variation
IDV(10)	C feed temperature (Stream 4)	Random variation
IDV(11)	Reactor cooling water inlet temperature	Random variation
IDV(12)	Condenser cooling water inlet temperature	Random variation
IDV(13)	Reaction kinetics	Slow drift
IDV(14)	Reactor cooling water valve	Sticking
IDV(16)	Unknown	Unknown
IDV(17)	Unknown	Unknown
IDV(18)	Unknown	Unknown
IDV(19)	Unknown	Unknown
IDV(20)	Unknown	Unknown
IDV(21)	Valve fixed at steady-state position	Constant position

A widely used dataset of TE process can be found in <http://web.mit.edu/braatzgroup/links.html> (accessed on 25 September 2023). In this study, we also adopt this dataset. Specifically, 22 measured variables XMEAS(1:22) and 11 manipulated variables XMV(1:11) are selected as $\mathbf{x} \in \mathbb{R}^{33}$. 500 samples collected under the normal operating condition (IDV(0)) are used as a training dataset. For each faulty dataset, it has 960 samples in total where the fault is injected from the 160th sample.

To assess the fault detection performance, three indices including missed detection rate (MDR), detection delay (DD), and false detection rate (FAR) are used. DD is defined as the time interval from the start of the fault to the detection time, which is expressed as the first time of five consecutive rises. MDR and FAR with a 99.9% confidence level can be calculated as follows:

$$\text{MDR}(\%) = \frac{\text{No. of samples}(J \leq J_{UCL} | \text{Fault})}{\text{total samples}(\text{Fault})} \times 100\%$$

$$\text{FAR}(\%) = \frac{\text{No. of samples}(J > J_{UCL} | \text{Normal})}{\text{total samples}(\text{Normal})} \times 100\%$$

where $J \in \{T^2, Q\}$ and $J_{UCL} \in \{T_{UCL}^2, Q_{UCL}\}$.

For a comparative study, several typical fault detection methods including PCA, NPE, LPP, principal component pursuit (PCP) [34], kernel PCA (KPCA) [35], mixed KPCA (MKPCA), structured joint sparse PCA (SJSPCA) [36], LE, LLE, and HLLE are employed. For PCA, $d = 19$ is set according to the 95% cumulative percentage of variance (CPV). For the NPE, $k = 5$ and $d = 19$ are selected. For LPP, $k = 5$, $\delta = 1650$, and $d = 19$ are selected. For PCP, $d = 19$ is selected. For KPCA, the kernel widths $C = 1000$ and $d = 22$ are selected. For MKPCA, the kernel widths C_1 and C_2 are set as 500 and 1000, respectively, and $d = 28$ is selected. For SJSPCA, $k = 5$, $\lambda_1 = 600$, $\lambda_2 = 50$, and $d = 19$ are selected. As displayed in Figure 2, $k = 5$ is selected for the TE case. Similarly, as shown in Figure 3, $c_1 = 0.25$ and $c_2 = 0.25$ are chosen. For LE, LLE, and HLLE, $\delta = 1650$, $d = 19$. For FLML, $\delta = 1650$, $c_1 = 0.25$, $c_2 = 0.25$, and $d = 19$ are selected.

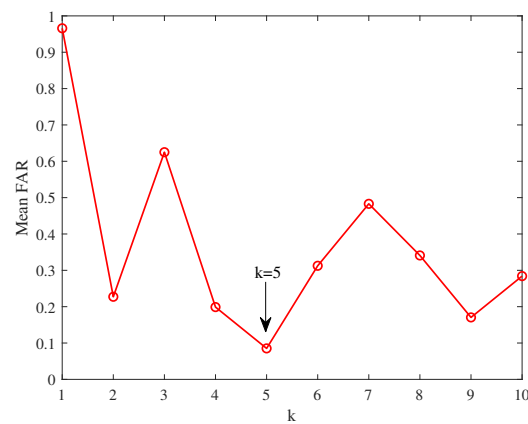


Figure 2. Mean FAR with different k for the TE process.

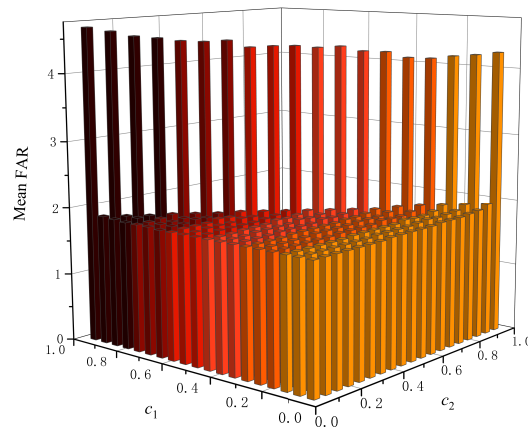


Figure 3. Grid search result of the fusion weights c_1 and c_2 for the TE process.

Tables 2 and 3 list the MDRs and FARs of 18 faults. It can be observed that the NPE and LPP can provide superior performance over PCA. The utilization of local structure information can enhance fault detection performance. On the other hand, FLML T^2 statistic offers the lowest MDRs among all the comparative methods. The average of MDRs of FLML T^2 statistic is 7.58%. Compared to LE, LLE and HLL methods, the average of MDRs of FLML T^2 statistic is increasingly reduced. Furthermore, the FARs of FLML T^2 statistics reach the same level of LE, LLE, and HLL. The average of FARs of FLML T^2 statistics is 0.21%. The DD index represents the sensitivity of monitoring statistics. A smaller DD means the monitoring statistic can detect the fault earlier. Table 4 lists the DDs for all methods, where the DD is indicated in the unit of the hour. As displayed in Table 4, the FLML T^2 statistic almost derives the smallest DD among the all methods.

To further illustrate the superiority of the proposed FLML method, the monitoring results are depicted in Figures 4 and 5 by PCA, NPE, LPP, PCP, KPCA, MKPCA, SJSPCA, and FLML methods for IDV (10) and IDV (19), respectively. Fault 10 is designed by adding a random disturbance on the C feed temperature (Stream 4). Compared to the step type fault scenarios such as fault 1 or fault 2, fault 10 is more difficult to detect. As shown in Figure 4, it is observed that FLML T^2 can detect most of the faulty samples. In contrast, other monitoring statistics such as PCA T^2 , NPE T^2 , PCP T^2 , KPCA T^2 , MKPCA T^2 , SJSPCA T^2 , and LPP T^2 cannot effectively detect the fault 10, since most of the monitoring statistics are below the corresponding UCLs. Fault 19 is an unknown faulty type. The monitoring results of fault 19 are displayed in Figure 5. By comparison, it can be observed that PCA, NPE, LPP, PCP, KPCA, MKPCA, and SJSPCA fail to detect the occurrence of fault 19. The online statistics are almost lower than the UCLs after the 161th sample. A promising result can be obtained using FLML T^2 , as shown in Figure 5h.

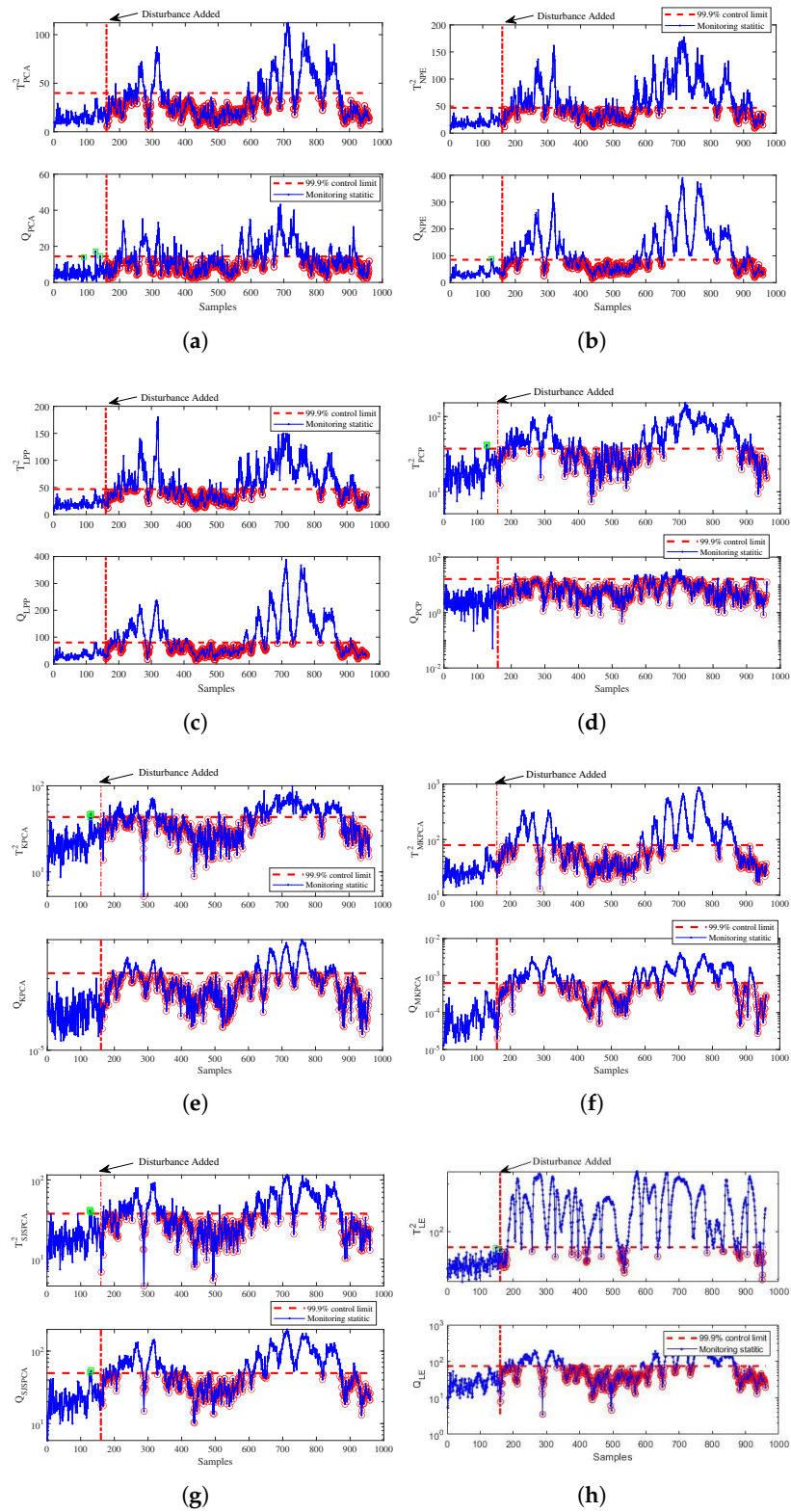


Figure 4. Cont.

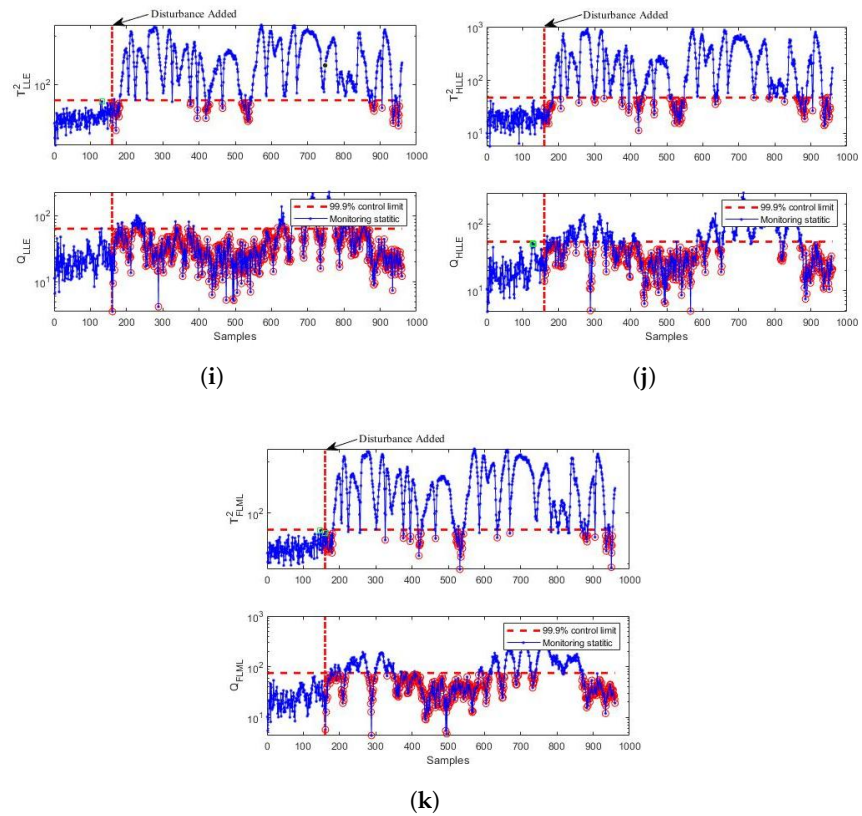


Figure 4. Monitoring results for the fault 10: TE process. (a) PCA; (b) NPE; (c) LPP; (d) PCP; (e) KPCA; (f) MKPCA; (g) SJSPCA; (h) LE; (i) LLE; (j) HLL; (k) FLML.

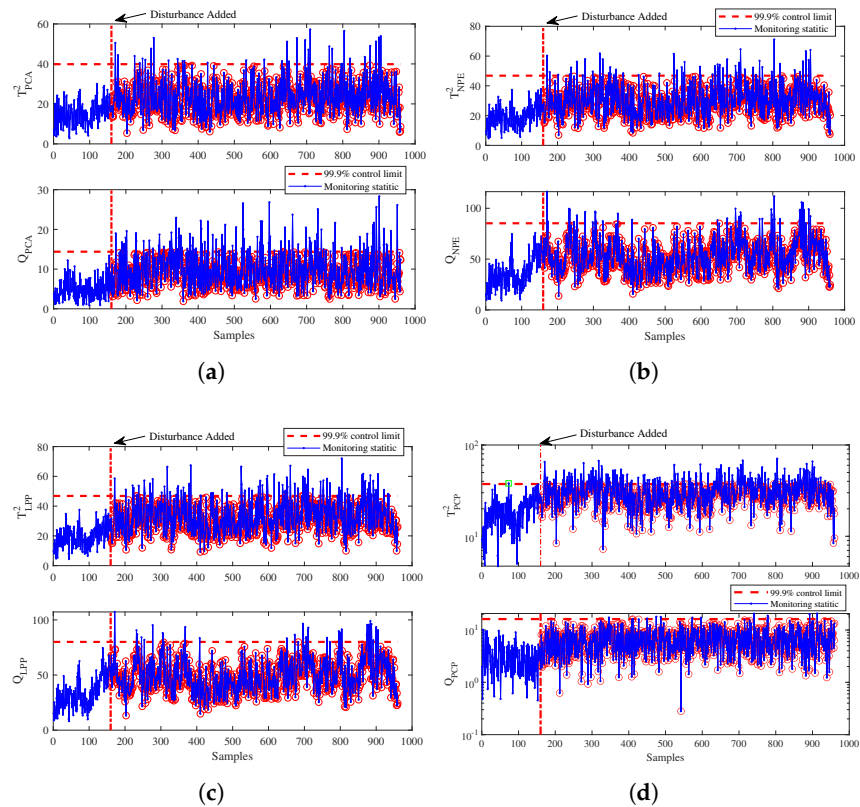


Figure 5. Cont.

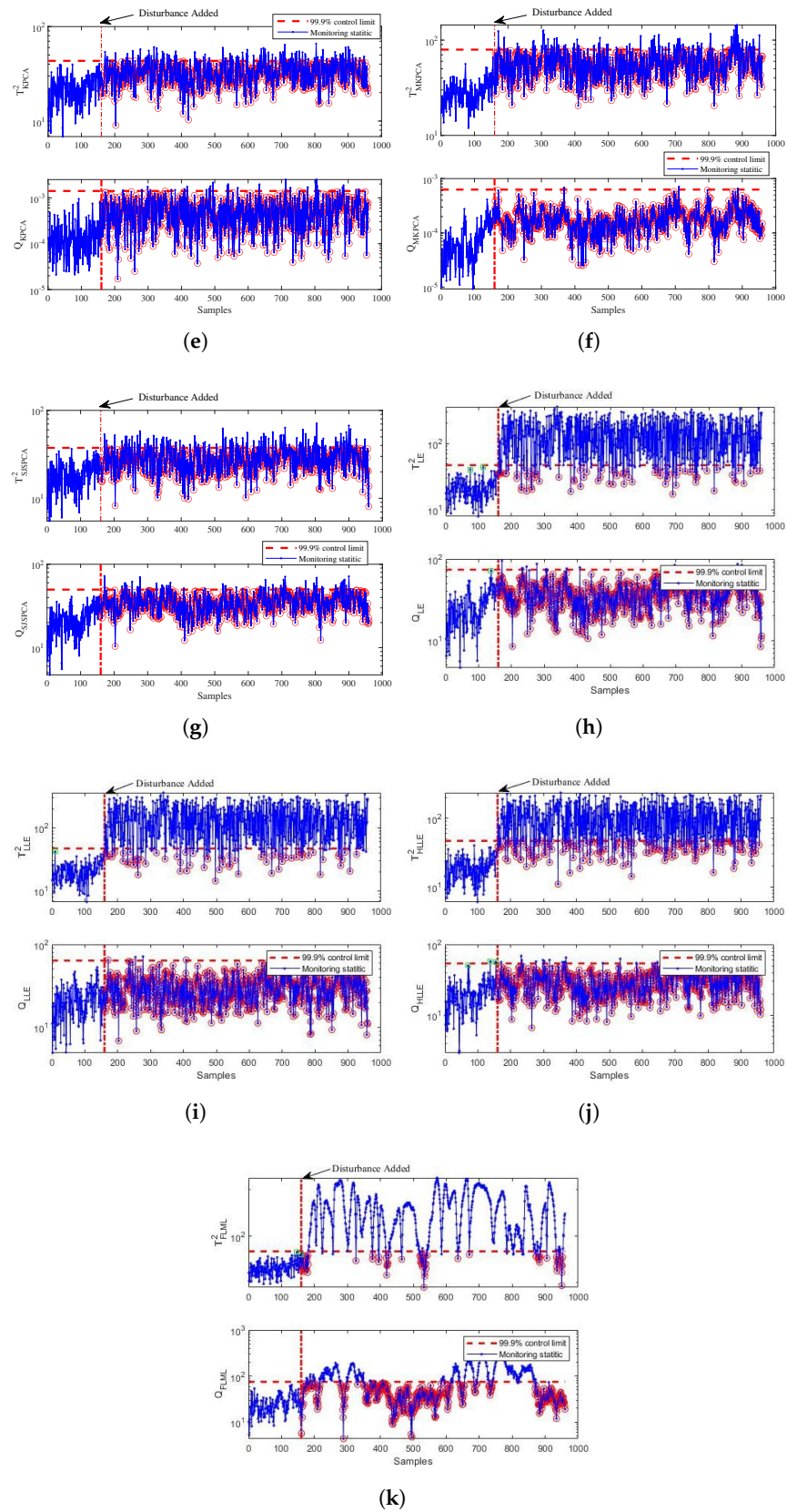


Figure 5. Monitoring results for the fault 19: TE process. (a) PCA; (b) NPE; (c) LPP; (d) PCP; (e) KPCA; (f) MKPCA; (g) SJSPCA; (h) LE; (i) LLE; (j) HLL; (k) FLML.

4.2. Blast Furnace Ironmaking Process

In this section, the proposed method is verified through a real blast furnace (BF) ironmaking process at a steel company in South China. In the steel manufacturing process, the blast furnace ironmaking process plays a vital role. The blast furnace ironmaking process is considered one of the most complex industrial processes. The basic units of the blast furnace ironmaking process are depicted in Figure 6. As it can be seen from Figure 6, the ironmaking process can be mainly divided into several sub-systems including the charging system, gas processing system, hot air system, the pulverized coal injection system, the iron system, and the BF body. The inner structure of the blast furnace is vertical. In the BF, the iron ore and coke are fed from the top along the vertical direction. The 1000 °C hot air and coal powder are blown into the furnace from the bottom. Through complex chemical reactions, the molten iron and slag are generated and accumulated in the hearth. In a periodical way, the molten iron and slag are discharged from the bottom of the furnace through the tap hole. As a byproduct, the flux gas escapes from the top of the furnace.

In the ironmaking process, it often suffers from abnormal furnace conditions, due to the effects of unreasonable daily operation and various disturbances. If these abnormal furnace conditions are not detected in a timely manner, the product quality will be degraded, and even the safety of the plant may not be ensured. Thus, the effective detection of abnormalities becomes an indispensable component of the operation of a blast furnace. In this study, we consider the detection of the channeling fault. The channeling fault may be caused by several reasons such as the low-quality coke pulverized coal or the inappropriate adjustment of air volume. In a channeling accident, the high-temperature furnace gas passes in the path of least resistance at a high velocity. The furnace gas increases the heat load at the wall and top of the furnace, resulting in possible equipment damage such as burning of the bag dust catcher [37].

In this case, a dataset was collected from 21 December 2013 to 5 January 2014. The sampling interval is 10 s. As demonstrated in [38], we select seven variables that are the most sensitive to faults. These variables are listed in Table 5. A total of 1000 samples are collected from 21 December 00:20 to 20–28 December 09:40 under the normal operating conditions as the training dataset. According to the accident report of the operation personnel, from 30 December 2013 23:44 to 31 December 2013 05:18, the ironworks accident report recorded the occurrence of the channeling. To facilitate the verification of fault detection performance, a testing dataset is generated, wherein 1200 samples were collected where the fault occurred from the 200th sample.

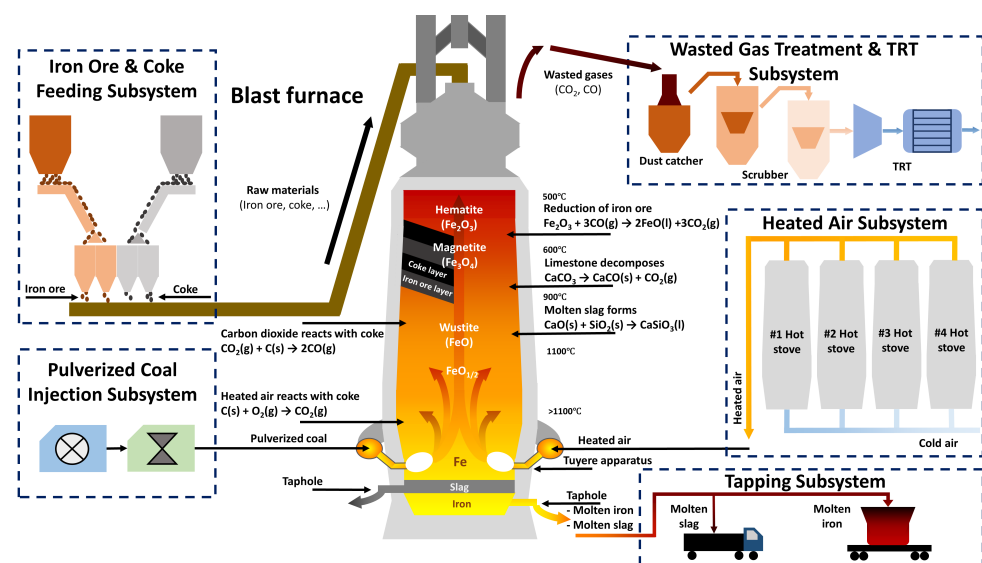


Figure 6. Diagram of blast furnace ironmaking process [39].

Table 5. Variable description of the blast furnace ironmaking process.

No.	Variable Description	Unit
1	Oxygen enrichment rate	%
2	Enriching oxygen flow	(m ³ /s)
3	Hot blast temperature	°C
4	Top temperature (1)	°C
5	Top temperature (2)	°C
6	Top temperature (3)	°C
7	Downcomer temperature	°C

For PCA, $d = 3$ is selected. For NPE, the neighbor parameter k and number of principle components d are selected to be 5 and 3, respectively. For LPP, $k = 5$, $d = 3$, and $\delta = 7 \times 50$ are determined. For PCP, $d = 4$ is selected. For KPCA, $C = 200$ and $d = 3$. For MKPCA, $C_1 = 150$, $C_2 = 200$ and $d = 3$. For SJSPCA, $k = 5$, $\lambda_1 = 600$, $\lambda_2 = 50$, and $d = 3$. For fair comparison, $k = 5$, $d = 3$, $\delta = 7 \times 50$ are selected for LE, LLE, HLLE, and FLML. The result of grid search for selecting c_1 and c_2 is plotted in Figure 7. On the basis of grid search results, $c_1 = 0.3$ and $c_2 = 0.3$ are determined.

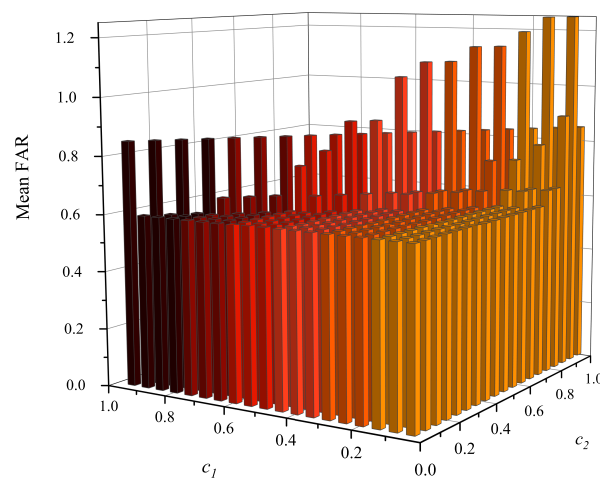


Figure 7. Grid search result of the fusion weights c_1 and c_2 for the blast furnace ironmaking process.

The monitoring results are plotted in Figure 8. It can be observed that NPE and LPP T^2 statistics can detect more faulty samples than the PCA T^2 statistic. But the improvement is limited, as shown in Figure 8. The reason for this may be that NPE and LPP only extract partial local structure information. It is also noticed that there are more false alarms for PCA Q and PCP Q statistics. Compared to the other methods, the proposed FLML method can provide much better performance, as shown in Figure 8h. Only a few faulty samples are missed. Table 6 lists the MDRs, FARs, and DDs. As shown in Table 6, the MDR and FAR of FLML T^2 are 2.80% and 0.00%, respectively. The DD of FLML T^2 is 0.17 min. The channeling condition can be timely and accurately detected by FLML T^2 . Among these comparative methods, the proposed FLML method can offer the best monitoring performance.

Table 6. Comparison results of MDR, FAR, and DD values for blast furnace ironmaking process.

PCA (%)		NPE (%)		LPP (%)		PCP (%)		KPCA (%)		MKPCA (%)		SJSPCA (%)		LE (%)		LLE (%)		HLLE (%)		FLML (%)	
T^2	Q	T^2	Q	T^2	Q	T^2	Q	T^2	Q	T^2	Q	T^2	Q	T^2	Q	T^2	Q	T^2	Q	T^2	Q
26.70	78.80	23.10	93.80	26.20	93.80	21.80	71.20	23.90	94.10	22.60	84.70	28.10	71.10	6.60	93.50	8.40	98.50	7.00	91.80	2.80	85.70
0.00	13.00	0.00	0.00	0.00	0.00	0.00	13.00	0.00	0.00	0.00	2.50	0.00	3.00	8.00	0.00	17.00	0.00	17.50	0.00	0.00	0.00
0.17	21.67	0.17	6.40	0.17	6.40	0.17	18.33	0.17	57.83	0.17	53.83	0.17	2.17	0.02	6.45	0.02	5.80	0.02	6.13	0.17	5.89

a: First row: missed detection rates (MDRs, %). b: Second row: false alarm rates (FARs, %). c: Third row: detection delays (DDs, mins).

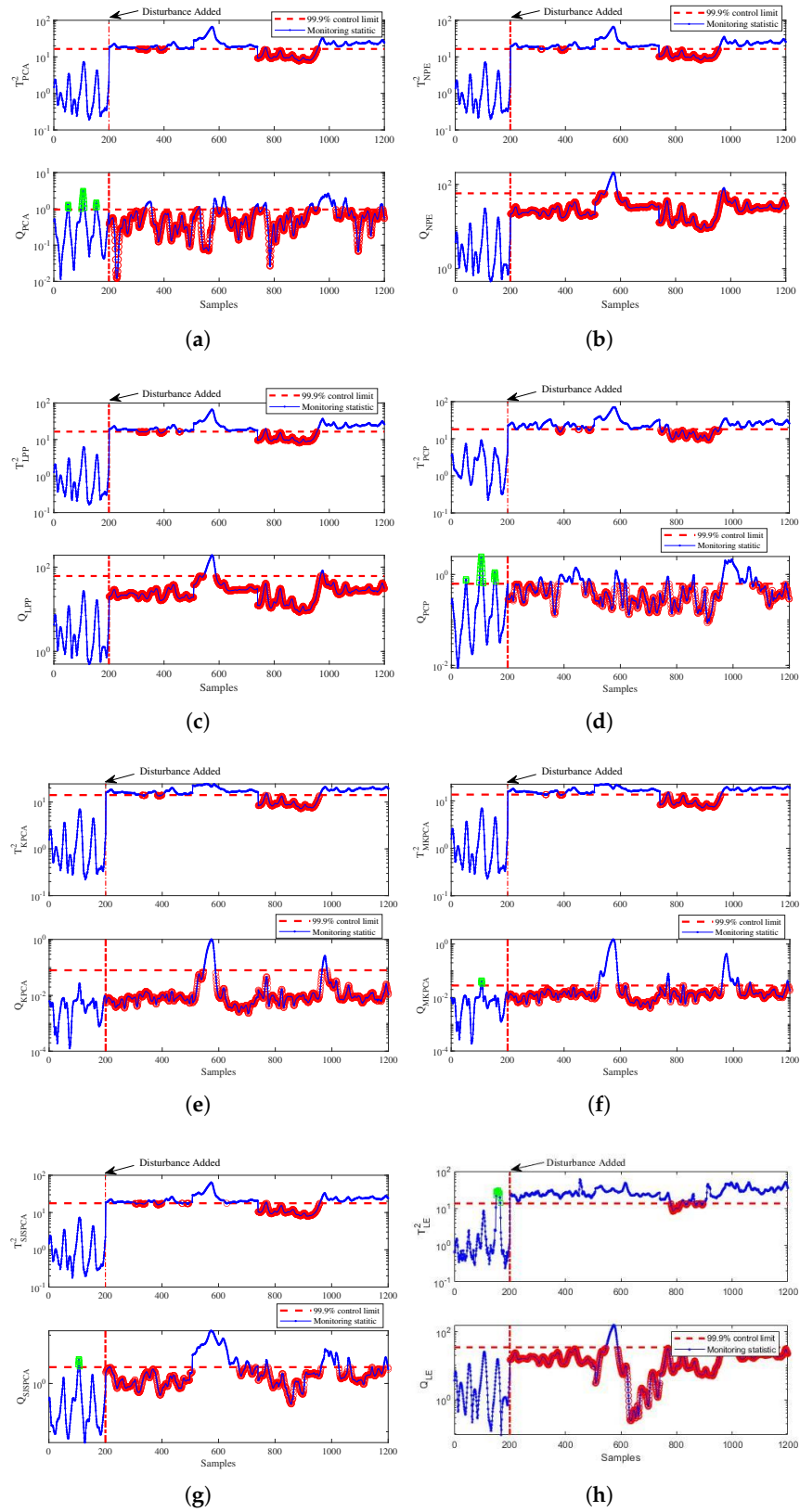


Figure 8. Cont.

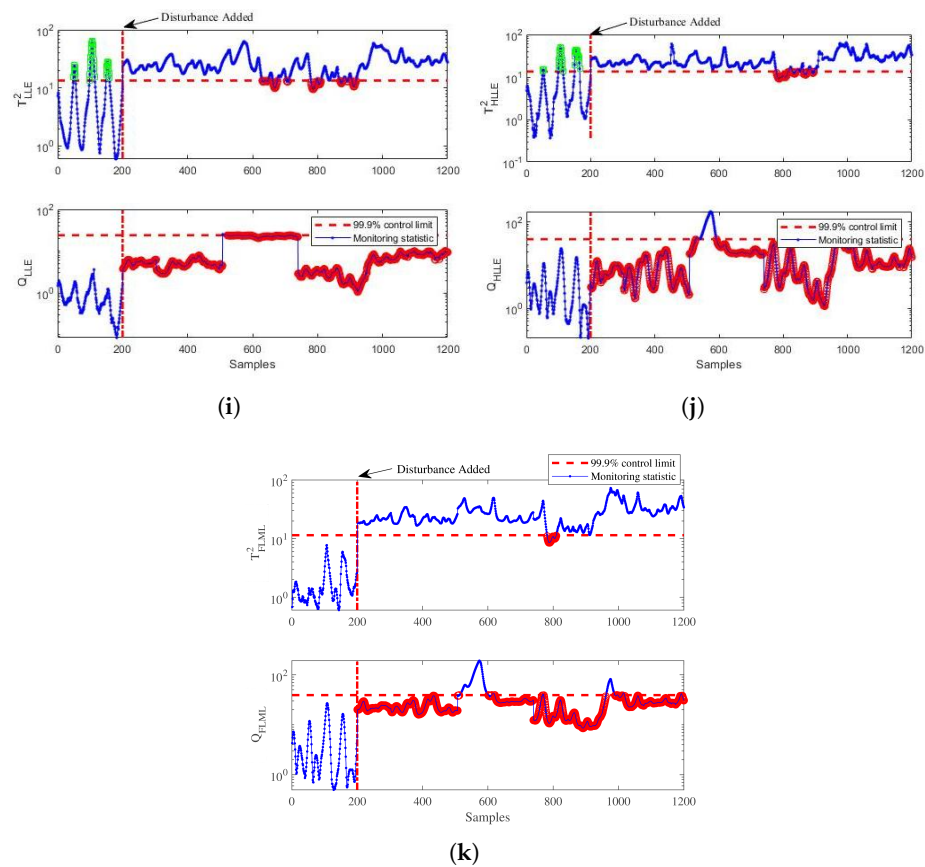


Figure 8. Monitoring results for the channeling condition: blast furnace ironmaking process. (a) PCA; (b) NPE; (c) LPP; (d) PCP; (e) KPCA; (f) MKPCA; (g) SJSPCA; (h) LE; (i) LLE; (j) HLLE; (k) FLML.

5. Conclusions

In this paper, a novel data-driven fault detection technique based on fusing local manifold learning methods is proposed for complex industrial processes. The proposed method aims to explore a more comprehensive local structure by synthesizing partial information learned from LE, LLE, and HLLE. With the exploit of local geometric structure, the process data are projected into a lower-dimensional space. Hotelling's T^2 and Q statistics are employed for fault detection. Case studies on the widely used TE process benchmark and a real blast furnace ironmaking process show the superior monitoring performance of the proposed methods, by comparison with other related methods. However, the proposed FLML still has limitations such as its process dynamics and hyper-parameters selection. Future work will focus on the following aspects:

- The proposed FLML method is extended into a dynamic version by using time-lag data to handle the dynamic characteristics of industry processes.
- Heuristic optimization methods such as genetic algorithm and particle swarm optimization are employed to determine the hyper-parameters efficiently.
- The proposed FLML method is used for fault identification and classification

Author Contributions: Conceptualization, P.W.; Methodology, P.W. and K.W.; Investigation P.W.; Writing—original draft, P.W., K.W. and S.L.; Writing—review and editing, P.W., H.P. and J.G.; Data Curation, K.W. and J.G. All authors have read and agreed to the published version of the manuscript.

Funding: This research was funded by the Zhejiang Province Public Welfare Technology Application Research Project (Grant No. LGF19F030004, LGG21F030015), and Open Research Project of the State Key Laboratory of Industrial Control Technology, Zhejiang University, China (No. ICT2023B19), and National Natural Science Foundation of China under Grant 61703371.

Data Availability Statement: The dataset of TE process can be found in <http://web.mit.edu/braatzgroup/links.html> (accessed on 25 September 2023).

Conflicts of Interest: The authors declare no conflict of interest.

References

1. Bahr, N.J. *System Safety Engineering and Risk Assessment: A Practical Approach*; CRC Press: Boca Raton, FL, USA, 2014.
2. Khan, F.; Rathnayaka, S.; Ahmed, S. Methods and models in process safety and risk management: Past, present and future. *Process Saf. Environ. Prot.* **2015**, *98*, 116–147. [[CrossRef](#)]
3. Nan, C.; Khan, F.; Iqbal, M.T. Real-time fault diagnosis using knowledge-based expert system. *Process Saf. Environ. Prot.* **2008**, *86*, 55–71. [[CrossRef](#)]
4. Venkatasubramanian, V.; Rengaswamy, R.; Yin, K.; Kavuri, S.N. A review of process fault detection and diagnosis: Part I: Quantitative model-based methods. *Comput. Chem. Eng.* **2003**, *27*, 293–311. [[CrossRef](#)]
5. Tidriri, K.; Chatti, N.; Verron, S.; Tiplica, T. Bridging data-driven and model-based approaches for process fault diagnosis and health monitoring: A review of researches and future challenges. *Annu. Rev. Control* **2016**, *42*, 63–81. [[CrossRef](#)]
6. Dai, X.; Gao, Z. From model, signal to knowledge: A data-driven perspective of fault detection and diagnosis. *IEEE Trans. Ind. Inform.* **2013**, *9*, 2226–2238. [[CrossRef](#)]
7. Yin, S.; Ding, S.X.; Xie, X.; Luo, H. A review on basic data-driven approaches for industrial process monitoring. *IEEE Trans. Ind. Electron.* **2014**, *61*, 6418–6428. [[CrossRef](#)]
8. Qin, S.J.; Chiang, L.H. Advances and opportunities in machine learning for process data analytics. *Comput. Chem. Eng.* **2019**, *126*, 465–473. [[CrossRef](#)]
9. Wang, Y.; Zheng, D.; Jia, R. Fault diagnosis method for MMC-HVDC based on Bi-GRU neural network. *Energies* **2022**, *15*, 994. [[CrossRef](#)]
10. Yu, X.; Tang, B.; Deng, L. Fault diagnosis of rotating machinery based on graph weighted reinforcement networks under small samples and strong noise. *Mech. Syst. Signal Process.* **2023**, *186*, 109848. [[CrossRef](#)]
11. Velasco-Gallego, C.; Lazakis, I. RADIS: A real-time anomaly detection intelligent system for fault diagnosis of marine machinery. *Expert Syst. Appl.* **2022**, *204*, 117634. [[CrossRef](#)]
12. Yin, S.; Ding, S.X.; Haghani, A.; Hao, H.; Zhang, P. A comparison study of basic data-driven fault diagnosis and process monitoring methods on the benchmark Tennessee Eastman process. *J. Process Control* **2012**, *22*, 1567–1581. [[CrossRef](#)]
13. Dong, Y.; Qin, S.J. A novel dynamic PCA algorithm for dynamic data modeling and process monitoring. *J. Process Control* **2018**, *67*, 1–11. [[CrossRef](#)]
14. Yin, S.; Li, X.; Gao, H.; Kaynak, O. Data-based techniques focused on modern industry: An overview. *IEEE Trans. Ind. Electron.* **2014**, *62*, 657–667. [[CrossRef](#)]
15. Tenenbaum, J.B.; De Silva, V.; Langford, J.C. A global geometric framework for nonlinear dimensionality reduction. *Science* **2000**, *290*, 2319–2323. [[CrossRef](#)]
16. Roweis, S.T.; Saul, L.K. Nonlinear dimensionality reduction by locally linear embedding. *Science* **2000**, *290*, 2323–2326. [[CrossRef](#)]
17. Belkin, M.; Niyogi, P. Laplacian eigenmaps for dimensionality reduction and data representation. *Neural Comput.* **2003**, *15*, 1373–1396. [[CrossRef](#)]
18. Zhang, Z.; Zha, H. Principal manifolds and nonlinear dimensionality reduction via tangent space alignment. *SIAM J. Sci. Comput.* **2004**, *26*, 313–338. [[CrossRef](#)]
19. He, X.; Niyogi, P. Locality preserving projections. *Adv. Neural Inf. Process. Syst.* **2004**, *16*, 153–160.
20. He, X.; Cai, D.; Yan, S.; Zhang, H.J. Neighborhood preserving embedding. In Proceedings of the Tenth IEEE International Conference on Computer Vision (ICCV'05) Volume 1, Beijing, China, 17–21 October 2005; Volume 2, pp. 1208–1213.
21. Donoho, D.L.; Grimes, C. Hessian eigenmaps: Locally linear embedding techniques for high-dimensional data. *Proc. Natl. Acad. Sci. USA* **2003**, *100*, 5591–5596. [[CrossRef](#)]
22. Chen, H.; Wu, J.; Jiang, B.; Chen, W. A modified neighborhood preserving embedding-based incipient fault detection with applications to small-scale cyber-physical systems. *ISA Trans.* **2020**, *104*, 175–183. [[CrossRef](#)]
23. Song, B.; Ma, Y.; Shi, H. Multimode process monitoring using improved dynamic neighborhood preserving embedding. *Chemom. Intell. Lab. Syst.* **2014**, *135*, 17–30. [[CrossRef](#)]
24. Duan, Y.; Liu, M.; Dong, M. A Metric-Learning-Based Nonlinear Modeling Algorithm and Its Application in Key-Performance-Indicator Prediction. *IEEE Trans. Ind. Electron.* **2019**, *67*, 7073–7082. [[CrossRef](#)]
25. Zhang, M.; Ge, Z.; Song, Z.; Fu, R. Global-local structure analysis model and its application for fault detection and identification. *Ind. Eng. Chem. Res.* **2011**, *50*, 6837–6848. [[CrossRef](#)]
26. Wu, P.; Lou, S.; Zhang, X.; He, J.; Gao, J. Novel Quality-Relevant Process Monitoring based on Dynamic Locally Linear Embedding Concurrent Canonical Correlation Analysis. *Ind. Eng. Chem. Res.* **2020**, *59*, 21439–21457. [[CrossRef](#)]
27. Li, B.; Zhang, Y. Supervised locally linear embedding projection (SLLEP) for machinery fault diagnosis. *Mech. Syst. Signal Process.* **2011**, *25*, 3125–3134. [[CrossRef](#)]
28. Xing, X.; Wang, K.; Lv, Z.; Zhou, Y.; Du, S. Fusion of local manifold learning methods. *IEEE Signal Process. Lett.* **2014**, *22*, 395–399. [[CrossRef](#)]

29. Xing, X.; Du, S.; Wang, K. Robust hessian locally linear embedding techniques for high-dimensional data. *Algorithms* **2016**, *9*, 36. [[CrossRef](#)]
30. Bezdek, J.C.; Hathaway, R.J. Some notes on alternating optimization. In Proceedings of the AFSS International Conference on Fuzzy Systems, Calcutta, India, 3–6 February 2022; Springer: Berlin/Heidelberg, Germany, 2002; pp. 288–300.
31. Bernal-de Lázaro, J.; Llanes-Santiago, O.; Prieto-Moreno, A.; Knupp, D.; Silva-Neto, A. Enhanced dynamic approach to improve the detection of small-magnitude faults. *Chem. Eng. Sci.* **2016**, *146*, 166–179. [[CrossRef](#)]
32. Downs, J.J.; Vogel, E.F. A plant-wide industrial process control problem. *Comput. Chem. Eng.* **1993**, *17*, 245–255. [[CrossRef](#)]
33. Chiang, L.; Russell, E.; Braatz, R. *Fault Detection and Diagnosis in Industrial Systems*; Springer: Berlin/Heidelberg, Germany, 2001.
34. Candès, E.J.; Li, X.; Ma, Y.; Wright, J. Robust principal component analysis? *J. ACM* **2011**, *58*, 1–37. [[CrossRef](#)]
35. Lee, J.M.; Yoo, C.; Choi, S.W.; Vanrolleghem, P.A.; Lee, I.B. Nonlinear process monitoring using kernel principal component analysis. *Chem. Eng. Sci.* **2004**, *59*, 223–234. [[CrossRef](#)]
36. Liu, Y.; Zeng, J.; Xie, L.; Luo, S.; Su, H. Structured joint sparse principal component analysis for fault detection and isolation. *IEEE Trans. Ind. Inform.* **2018**, *15*, 2721–2731. [[CrossRef](#)]
37. Zhou, B.; Ye, H.; Zhang, H.; Li, M. Process monitoring of iron-making process in a blast furnace with PCA-based methods. *Control Eng. Pract.* **2016**, *47*, 1–14. [[CrossRef](#)]
38. Wang, L.; Yang, C.; Sun, Y.; Zhang, H.; Li, M. Effective variable selection and moving window HMM-based approach for iron-making process monitoring. *J. Process Control* **2018**, *68*, 86–95. [[CrossRef](#)]
39. Lou, S.; Yang, C.; Zhang, X.; Zhang, H.; Wu, P. Blast Furnace Ironmaking Process Monitoring With Time-Constrained Global and Local Nonlinear Analytic Stationary Subspace Analysis. *IEEE Trans. Ind. Inform.* **2023**, 1–14. [[CrossRef](#)]

Disclaimer/Publisher’s Note: The statements, opinions and data contained in all publications are solely those of the individual author(s) and contributor(s) and not of MDPI and/or the editor(s). MDPI and/or the editor(s) disclaim responsibility for any injury to people or property resulting from any ideas, methods, instructions or products referred to in the content.